Applied Catalysis A, General 670 (2024) 119529

Contents lists available at ScienceDirect

Applied Catalysis A, General

journal homepage: www.elsevier.com/locate/apcata

Design and performance testing of a monolithic nickel-based SiC catalyst for steam methane reforming

Ziqi Shen, Seyed Ali Nabavi, Peter T. Clough *

Energy and Sustainability Theme, Cranfield University, Cranfield, Bedfordshire MK43 0AL, UK

ARTICLE INFO

Keywords:
Structured catalysts
Silicon carbide
Monolith
Steam methane reforming
Hydrogen production

ABSTRACT

Hydrogen is a highly promoted carbon-free energy carrier that has drawn significant attention recently due to its potential to decarbonise energy sector. More than three-quarters of hydrogen is currently produced via steam methane reforming (SMR), and nickel-based catalysts are used in most applications. Structured catalysts have been reported to be able to further improve catalyst performance as they can optimise heat and mass transfer, as well as prevent coke formation with its structural and textural proprieties. Silicon carbide (SiC) has excellent hardness, thermal conductivity, and chemical inertness, therefore is a promising material to develop structured nickel-based monolithic SiC catalysts for SMR. In this work, a structured monolithic catalyst support has been formed by a modified freeze-gelation method, initially starting from SiC powder, and nickel has been distributed to form a monolithic nickel-based catalyst by wet impregnation. The results showed that the catalysts can achieve thermodynamic equilibrium at 600 °C with a gas hourly space velocity (GHSV) of 10,000 h^{-1}, while reaching a high methane conversion of 86% at 800 °C and GHSV value of 20,000 h^{-1} during the performance tests using low feeding concentration and low pressure. This is the first time SiC catalytic materials have had their performance demonstrated for SMR under realistic operating conditions.

1. Introduction

Hydrogen is an alternative to traditional energy carriers as it has high gravimetric energy density and does not release greenhouse gas emissions upon combustion. Therefore, it is expected to play a significant role in decarbonisation of energy sector if produced through low-carbon processes [1]. However, most of the 94 Mt of hydrogen produced annually was from fossil fuels via a mature technology – steam methane reforming (SMR) and resulted in a high amount of carbon dioxide is emitted at the same time [2]. This dominant process is based on the endothermic reforming of methane (Eq. (1)), the produced syngas then undergoes the water-gas shift reaction to upgrade the H_2 content (Eq. (2)):

$$CH_4 + H_2O \leftrightarrow CO + 3H_2 \Delta H^{\circ}_{298} = +206kJ \bullet mol^{-1} \quad (1)$$

$$CO + H_2O \leftrightarrow CO_2 + H_2 \Delta H^{\circ}_{298} = -41kJ \bullet mol^{-1} \quad (2)$$

In commercial applications, the SMR process typically requires severe conditions (800–1000 °C, 8–35 bar) using various catalysts filled in a fixed bed externally heated tubular reformer [3]. Also, the gas space velocity of industrial process was relatively high, usually greater than 10,000 h^{-1} for SMR [4]. Some physical and chemical properties of catalyst are critical to SMR, such as its metal content, porosity, and particle size, which are all optimised to improve process performance [5]. The most widely applied catalysts for SMR are nickel-based catalysts, due to nickel's relatively inexpensive price and good activity [6,7], and many studies have tried to improve its catalytic performance by additive doping, producing novel bi-metallic, multi-metallic catalysts or composites [8]. Researchers of SMR catalysts have mostly focussed on methane conversion and carbon monoxide selectivity and tend to only achieve low methane conversion and low hydrogen yield when utilising low operating temperature and pressure [9]. Some researchers have developed catalysts containing high content of nickel (over 60%) and reported a correspondingly high methane conversion and hydrogen yield, when the gas space velocity was great than 10,000 h^{-1}, however, the operating temperature remained high (over 800 °C) and the methane feed was pure [10]. Therefore, a novel nickel-based catalyst is needed, which can demonstrate good catalyst activity in terms of methane conversion and hydrogen yield for SMR, with a lower energy consumption, a lower cost, and a closer flow conditions to realistic

* Corresponding author.
E-mail address: P.T.Clough@cranfield.ac.uk (P.T. Clough).

https://doi.org/10.1016/j.apcata.2023.119529
Received 11 September 2023; Received in revised form 26 November 2023; Accepted 30 November 2023
Available online 2 December 2023
0926-860X/© 2023 The Author(s). Published by Elsevier B.V. This is an open access article under the CC BY license (http://creativecommons.org/licenses/by/4.0/).

process conditions.

Structured catalysts are innovative for catalyst development as they can help understand the relations of essential parts in the reaction [11], as SMR is a complex system containing momentum, materials, mass and heat balances. The monolithic catalysts have several advantages: (1) with the porous structure and channels, mass transport and mixing degree are enhanced, while material concentration differences can be axially evened without radial diffusion; (2) using high thermal conductive material, heat conduction is improved; (3) the pressure drop of monolithic reactors is low, depending on its structural design [12,13]. Also, some nickel-based catalysts were reported to inhibit coke formation under SMR due to its porous structure [14].

Materials choice is a key factor in catalyst design for SMR, and silicon carbide (SiC) is a highly feasible candidate material that can be synthesised into structured monoliths [11]. SiC exhibits many optimal physical and chemical properties, such as high thermal conductivity, high mechanical strength and chemical inertness [15,16]. SiC can play two different roles in a catalytic system: as a diluent / in-bed thermal ballast, for example, some researchers used SiC powder as a catalyst dilution agent to improve bed's heat transfer [17–19]; as a catalyst support, such as the SiC monoliths [20]. Formed with this material, structured SiC monoliths enable excellent axial and radial heat transfer [11], which is hard to achieve with conventional materials that are often low thermal conductivity ceramic materials, and the endothermic SMR process can benefit from these highly thermally conductive materials with a consequent improvement of its performance and reduction in heat transfer resistance and hot spot minimisation [21]. Meanwhile, structured SiC monoliths can maintain it highly porous structure during the SMR process as no thermal, mechanical shock and corrosion can occur or with minimum influence. Moreover, active metals including Pt, Rh, Ru and Ni were reported to have good stability on the surface of SiC [15,16]. Researchers chose SiC as the support materials of catalysts, designed for many different mechanisms including steam reforming of methane [1,21–25], propane [26,27], methanol [28–30], ethanol [31,32], or other reforming mechanisms, but they may only focus on the material.

In this work, a novel nickel based monolithic SiC catalyst was designed, prepared and tested for the SMR reaction. The design was focused on its controlled macroporous structure. To better understand how the structured monolithic catalyst works under SMR conditions, a fixed-bed reactor was used to evaluate its performance, under strict operating conditions: high space velocity, low feeding concentration, low temperature and pressure. The performance of the catalyst was then compared with other structured SiC catalysts in literature. The results showed that the monolithic catalysts can work efficiently in harsh but realistic operating conditions, especially at low SMR temperature, and performed better than other nickel-based structured SiC catalysts designed for steam methane reforming.

2. Experimental

2.1. Materials and catalyst preparation

Silicon carbide powder (alpha-phase, 99.8% metals basis) was purchased from Alfa Aesar and its mean particle size and surface area were 2 μm and 9–11 m^2/g, respectively. Aluminium oxide (alpha phase, 99.95% metals basis) and zirconium oxide (calcined, 99%) from Alfa Aesar were used as sintering aids. Gelatine (Type A) was purchased from Sigma Aldrich with a bloom number of 175.

The freeze-gelation method developed by Fukushima et al. [33] was applied for the catalyst support preparation with simplifications in mixing process. For the monolithic catalyst preparation, a 10 wt% gelatine solution was prepared under 35 °C with 200 rpm magnetic agitation. The gelatine can stock high content of water when it was dissolved into water at 30–35 °C. Sintering aids were primarily mixed with silicon carbide powder by the dry mixing method with a SiC:Al_2O_3:ZrO_2 mass ratio of 96:2.4:1.6 [33]. Then, this powder was slowly added into gelatine solution with a volumetric solid/solution ratio of 1:3, and the mixture was continuously agitated for another 10 min to obtain a homogenous slurry. The slurry was poured into a plastic mould (made by 3D printing) and then transferred immediately to a freezer and frozen at − 18.5 °C overnight and then lyophilised at − 50 °C and 0.1 mbar for 48 h. Small ice crystals were formed and it can be used as the sacrificed templates to create pores [34]. After removing from the plastic mould, the dry monolith was calcined in air at 600 °C in a muffle furnace for 4 h (heating rate 1 °C·min^{-1}) to remove all organic compounds [33]. Finally, the calcinated monolith was sintered under nitrogen at 1400 °C in a tubular furnace for 4 h (heating rate 5 °C·min^{-1}) [35]. 'SiC-M' was used to denote the SiC monoliths.

The wet impregnation technique was chosen to deposit NiO crystallites over the monolithic SiC support (SiC-M) because of its ability to achieve an even coating across the pore surface area. For single monolith impregnation, 1.59 g, 7.95 g or 15.91 g of Nickel(II) nitrate hexahydrate ($Ni(NO_3)_2$•6 H_2O, 99%, Thermo Scientific) was transferred into a beaker and dissolved in 49.41 g, 47.05 g or 44.09 g of deionized water to create a precursor solution with a desired concentration (2 wt%, 10 wt% or 20 wt%, respectively). The monolith was then immersed inside the precursor solution with the help of a vacuum pump for 1 min until no air bubbles came out and impregnated in the same solution at 80 °C for 6 h with 100 rpm agitation to avoid impacting its structure. After impregnation, the monolith was dried overnight at 80 °C and then calcined at 600 °C in a muffle furnace for 4 h (heating rate 5 °C·min^{-1}). Depending on the concentration of precursor solutions, '2Ni/SiC-M', '10Ni/SiC-M' and '20Ni/SiC-M' were used to denote the monolithic catalysts prepared with 2 wt%, 10 wt% and 20 wt% solutions, respectively. The monolithic catalysts were denoted as 'xNi/SiC-M' which *x* refers to the precursor concentration (x = 2, 10, 20). Metal loading was evaluated using mass balance of coating agent before and after the thermal treatment of impregnated samples.

2.2. Catalyst characterisation

The volumetric density of SiC-M was evaluated using its definition (Eq. (3)) considering both monolith and pores inside. SiC-M monolith was formed into a cylindrical shape with dimensions of 20.2 ± 0.18 mm diameter and 16.8 ± 0.20 mm height.

$$\rho_{monolith} = \frac{m_{monolith}}{V_{monolith}} \tag{3}$$

The nickel loading of Ni/SiC-M catalysts were evaluated using the mass balance of nickel before and after calcination of the catalysts, by assuming nickel nitrate on surface of SiC-M was completely decomposed to be nickel oxide, and no change in composition of SiC-M supports.

Mercury intrusion porosimetry (MIP) was applied to measure porosity, pore size distributions and pore structural proprieties using a Micrometric AutoPore IV 9500. Nitrogen adsorption isotherms were obtained at 77 K using 3P Meso 222 to estimate Brunauer, Emmett and Teller (BET) specific surface area of SiC-M and fresh catalysts. Scanning electron microscopy (SEM) coupled with energy dispersive X-ray spectroscopy (EDS) were conducted using Tescan Vega 3 instrument at 20 kV to obtain the morphology data of catalyst supports and metal surface distribution of fresh and spent catalysts. X-ray powder diffraction (XRD) was also performed with a Siemens D5005 diffractor to evaluate the different phases and crystallite structural data of catalysts. The scanning was performed with 2θ varying between 5° and 90° with a step of 1.2°·min^{-1}. Temperature programmed reduction (TPR) was carried out with TA SDT 650 model. Around 30 mg sample was treated under a flow of 1.5% of H_2 (balanced with N_2) with a flow rate of 83 mL·min^{-1} and the operating temperature range was between 200 and 800 °C with a heating rate of 10 °C·min^{-1}.

2.3. Catalytic performance test

A fixed-bed reactor was used to evaluate the catalytic activity and performance of monolithic nickel based SiC ceramic catalysts. A gas feeding system, a steam generation system, a gas cooling and drying system, a control system and a gas measurement system were also connected to the reactor. The reactor configuration is shown in Fig. 1.

A gas mixture of 10% of methane (balanced with nitrogen) from BOC was used as the feedstock for catalytic tests, while another gas mixture of 10% of hydrogen (balanced with nitrogen) from BOC was used for in-situ catalyst activation. Three mass flow controllers (Bronkhorst UK) were used to introduce the gases (N_2, CH_4/N_2, H_2/N_2) into the reactor. A high-performance liquid chromatography (HPLC) pump (Jasco, model PU1586) was used to introduce deionised water to a steam generator and N_2 was used as the carrier gas. The sample was placed in the centre of reactor in an inert quartz liner, two layers of quartz wool (bottom and top) were used to keep the catalyst in position. Bed temperature was monitored by a K-type thermocouple and was operated in the range of 600 and 800 °C depending on the test being performed. All gases were preheated and maintained at over 100 °C to prevent condensation. Steam concentration was cross checked by measuring relative humidity with a humidity probe (Vaisala HMT330 series).

The exhaust gas was cooled down by a water-cooled condenser and the remaining moisture was removed with a $CaCl_2$ packed bed. A sample of the dried gas was sent to the gas measurement system consisting of two continuous multi-gas analysers (ADC MGA3000 model) to determine gas composition of CH_4, CO, CO_2 and H_2. These analysers were able to measure the gas composition at the gas analyser almost in real-time (response time ~4 s) at one second intervals.

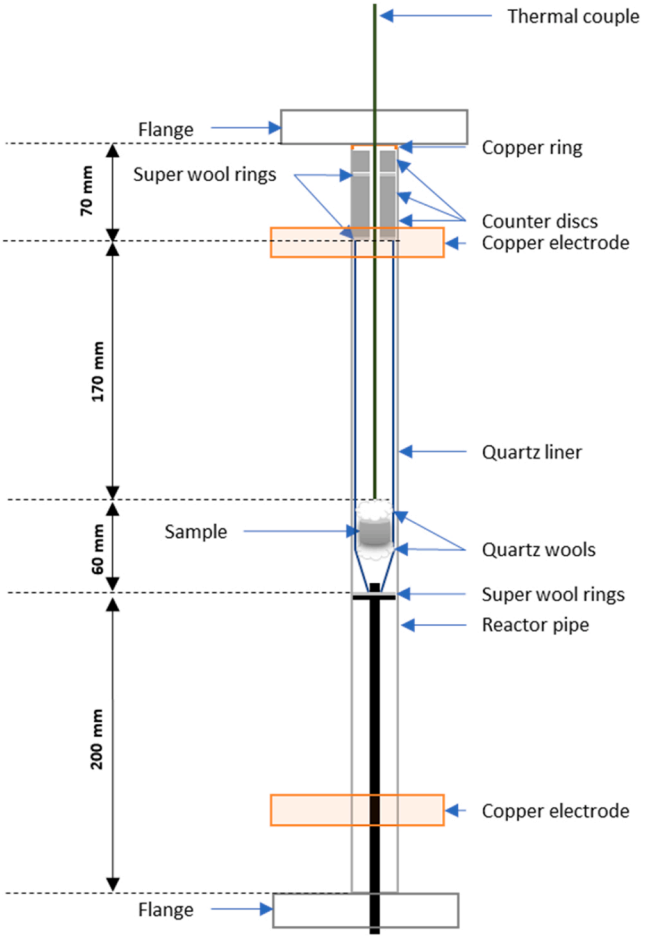


Fig. 1. Fixed bed reactor configuration utilised in this study.

In this work, samples were activated by 10% H_2 in N_2 at 600 °C until no water is generated. Each test was conducted with a fixed molar steam/carbon ratio of 3, and the pressure of gases were maintained at 1 bar. The in-situ gas hourly space velocity (GHSV) was calculated as gas flow rate per total volume of monolithic catalysts and controlled in each test, varying from 10,000 to 25,000 h^{-1}. These GHSV values represented relatively high space velocities in the fixed bed system but were selected to represent realistic operating conditions within a reformer. A table summed up the operating conditions of different samples and gas space velocity was given as below (Table 1).

Methane conversion (X_{CH_4}), hydrogen yield (y_{H_2}), hydrogen selectivity (s_{H_2}) and carbon monoxide selectivity (s_{CO}) were calculated using (Eqs. (4–7)):

$$CH_4\ conversion\ (\%) = \frac{F_{CH_{4,in}} - F_{CH_{4,out}}}{F_{CH_{4,in}}} \times 100\% \quad (4)$$

$$H_2\ yield\ (\%) = \frac{F_{H_{2,out}}}{4 \bullet F_{CH_{4,in}}} \times 100\% \quad (5)$$

$$H_2\ selectivity\ (\%) = \frac{F_{H_{2,out}}}{F_{H_{2,out}} + F_{CO_{out}} + F_{CO_{2,out}}} \times 100\% \quad (6)$$

$$CO\ selectivity\ (\%) = \frac{F_{CO_{out}}}{F_{CO_{out}} + F_{CO_{2,out}}} \times 100\% \quad (7)$$

In which $F_{i,in}$ and $F_{i,out}\left(i = CH_4, H_2, CO_2, CO\right)$ represent the molar flowrate of gas species *i* in the feeding and exhaust streams.

3. Results and discussion

3.1. Characterisation of catalysts

3.1.1. Volumetric density of monoliths and nickel loading

The fresh SiC ceramic support (SiC-M) was grey in appearance with pores and channels visible on the surface, and after impregnation it maintained its shape but the colour darkened slightly. The SiC-M can float on the surface of DI water as the volumetric density of SiC-M was found to be 0.33 ± 0.014 g/cm^3, which was about one third of water (0.997 g/cm^3 at 25 °C).

Table 2 shows the amount of nickel oxide coated on the surface of monoliths for two different precursor concentrations used for further tests. The nominal nickel contents are equal to the concentration of nickel precursor used for impregnation. For 20Ni/SiC-M, 3 samples were prepared and used to calculated absolute nickel loading. The nickel loading was 0.41 ± 0.018 g (in NiO) and 21.4 ± 0.5% (in wt% NiO). These results showed that the applied wet impregnation method was able to distribute nickel on the surface of SiC-M steadily. However, it was difficult to achieve the same loading of nickel in impregnation solution when it was used to prepare 10Ni/SiC-M and 2Ni/SiC-M.

3.1.2. Porosimetry of monoliths

Some critical structural and textual properties of SiC-M was shown in Fig. 2. SiC-M was highly porous and exhibited a complex structure between pores and channels. For mass transportation, the permeability

Table 1
Operating conditions of catalytic activity tests.

Samples	Nominal nickel loading (wt% $_{NiO}$)	GHSV (h^{-1})[a]
2Ni/SiC-M	2	20,000
10Ni/SiC-M	10	20,000
20Ni/SiC-M	20	25,000
		20,000
		15,000
		10,000

[a] The gas hourly space velocities were calculated using ideal gas equation.

Table 2
Nickel loadings on SiC monoliths.

Nickel solution concentration (wt%)	Amount of nickel (g_{NiO})	Amount of nickel (wt% $_{NiO}$)
2	0.02	1.3
10	0.17	9.2
20	0.41	21.4

and tortuosity data showed that the SiC-M may have a high pressure drop, but that may also lead to a longer contact time of gas compounds with active sites on the surface of materials once nickel was loaded. Fig. 2 also shows the pore size distribution of SiC-M indicating a largely macro-porous structure designed to assist with mass transport of the products and reactants.

3.1.3. Specific surface area of monoliths and catalysts

The specific BET surface areas (m^2/g) of SiC-M and various stages of the 20Ni/SiC-M catalysts are shown in Table 3. Silicon carbide has been claimed as a 'low surface area' material by others [36], herein, the BET surface area of SiC-M was comparable with the fresh SiC powder (9–11 m^2/g). It was observed that the BET surface area of SiC ceramic support decreased by nearly 30% after nickel metal was dispersed onto the surface via the wet impregnation. This can be explained by the possible blockage of open pores or channels by nickel crystallites [37]. The decrease of the BET surface area of reduced 20Ni/SiC-M can be explained by the possible variation of textural properties when NiO transformed to active nickel. The used catalysts seemed not to be deactivated as the surface area of the used 20Ni/SiC-M had no significant change compared to the reduced catalysts.

3.1.4. Morphology of monoliths and catalysts

SEM images of SiC-M were shown in Fig. 3(a), (b) and (c). The images confirmed that highly porous structures were successfully created by the modified freeze-gelation method, with pores and the surface connected by structured tunnels. Pore sizes ranged from 70 to 140 μm, which was smaller than the range of pore size found by Fukushima et al. (147 μm in average) [33]. Also, it can be observed that the surface of pores and channels among the SiC-M was coarse (Fig. 3(c)), which may facilitate the dispersion of metal on the surface. The rough surface of these giant pores may explain the non-conformality of pore size data obtained from MIP, as giant pores (70–140 μm) were easier to be destroyed during the preparation and measuring process of MIP.

It can be observed that the porous and coarse structure was maintained after NiO was added to the surface (Fig. 3(a), (b), (c) and (d)). It seems that the transformation of NiO to Ni active metal via H_2 reduction and the steam methane reforming reaction had certain surface textural impact over the catalysts' morphology (Fig. 3(d), (e) and (f)), as 'spherical' humps between 10 and 30 μm were found on the surface. Fig. 3(b) and (e) showed similar appearance with the presence of 'spherical' humps. The NiO layer may evenly encapsulate SiC monolith when catalysts were not activated or used, and the morphology of NiO layer obscured the morphology of monolithic support. After activation or reforming under high temperature (600–800 °C), nickel nanoparticles were sintered or deviated from the surface of monolith and the morphology of SiC monolith could reappear.

In Fig. 4, the mapping data highlighted the homogeneous distribution of NiO crystallites over not only the outer surface but also inner pores of SiC ceramic support, for both fresh and used catalysts. Although there was no additional oxidation stage to regenerate the spent catalysts, silicon dioxide was found over the surface. It may be able to explain the different morphology after the SMR process, as the oxygen from steam at high operating temperatures can trigger SiC to form silicon oxide, but only on the surface. In fact, SiC was found to react with steam to form amorphous silica and methane via the reaction below (Eq. (8)), especially at reaction temperature above 500 °C and high pressure [38]:

$$SiC + 2H_2O \rightarrow SiO_2 + CH_4 \quad (8)$$

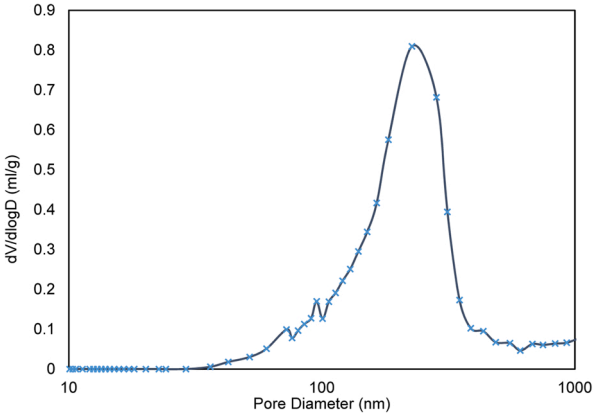
The oxidation of SiC in steam at 600–800 °C was likely to happen on surface of monolith and the most fragile part of the structure was collapsed and the 'spherical' humps were made. These humps contained a clump of SiC microcrystals (formed through Ostwald ripening) with a thin layer of silicon oxide on the surface. The formation and growth of SiC microcrystals by Ostwald ripening mechanism under high temperatures was also reported by Peng et al. [39], resulting in a variation in morphology.

3.1.5. Crystallography of monoliths and catalysts

Powder X-ray diffraction patterns of SiC-M, fresh 20Ni/SiC-M catalyst, reduced 20Ni/SiC-M and used 20Ni/SiC-M catalyst was obtained and are shown in Fig. 5. The XRD profile of the SiC ceramic support showed that α-SiC (2θ = 34.1, 35.6, 38.1, 41.3, 54.6, 60.0, 65.6, 71.7 and 73.3°) has a hexagonal structure, as the preparation process had no effect on SiC structure. The XRD pattern of fresh 20Ni/SiC-M catalysts showed that the appearance of NiO (2θ = 37.2, 43.3, 62.8, 75.4 and 79.4°) over SiC-M. Metallic nickel particles (2θ = 44.4, 51.7 and 76.2°) were found in the XRD data of the catalysts after reduction, revealing that the metal sites were fully activated and the structured SiC-M

Table 3
Surface properties of catalyst support and catalysts.

	SiC-M	Fresh 20Ni/SiC-M	Reduced 20Ni/SiC-M	Used 20Ni/SiC-M
S_{BET} (m^2/g)	11.26	8.01	6.52	6.91



Sample	SiC-M
Porosity (%)	78.4
Permeability (mDa)	183.4
Tortuosity	19.25
Average pore diameter (nm)	764

Fig. 2. Pore size distribution of catalyst support and its structural and textual properties.

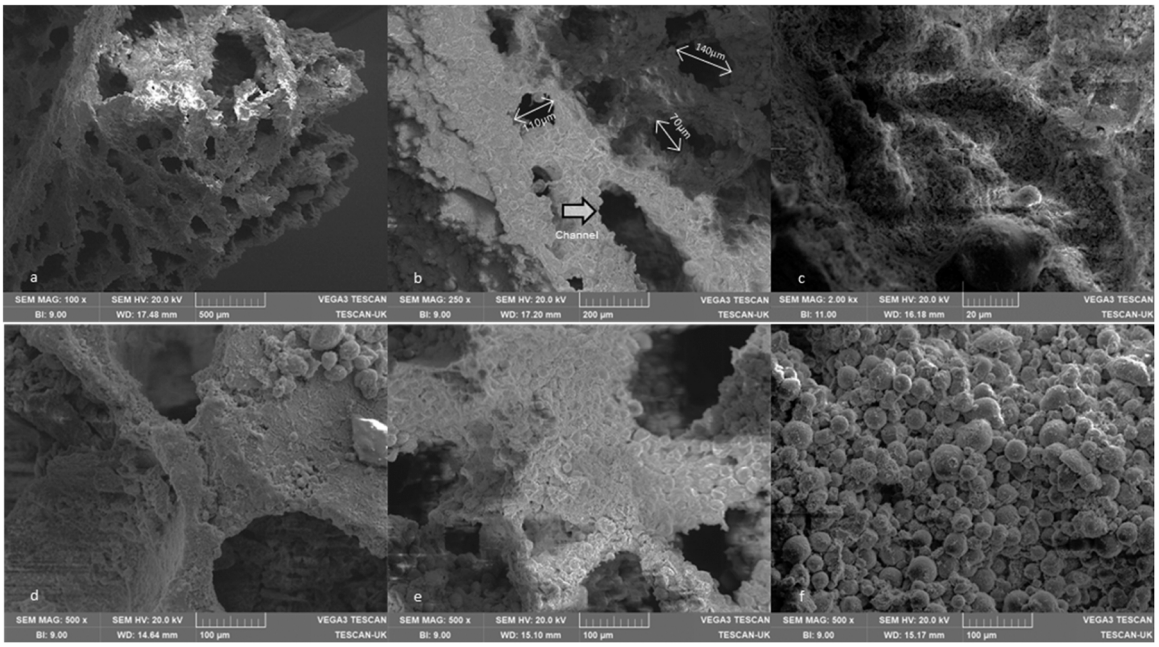


Fig. 3. SEM images of (a, b, c) monolithic SiC ceramic supports,(d) fresh catalysts, (e) reduced catalysts, and (f) used catalysts.

catalyst were allowed to be fully reacted with hydrogen through its pores and channels. The similar XRD profiles of the ceramic support (2θ = 34.1, 35.6, 38.1, 41.3, 54.6, 60.0, 65.6, 71.7 and 73.3°) and metallic nickel particle (2θ = 44.4, 51.7 and 76.2°) were identified from the XRD for used 20Ni/SiC-M after 1 h SMR test, by the comparison with the pattern of the reduced catalyst, there was no significant difference in terms of material phases, showing a stable and sustainable structure of catalysts during SMR. According to Scherrer's law, the mean crystallite size of NiO for fresh catalysts was calculated and was approximately 36.4 nm, and the mean crystallite size of nickel nanoparticles after reduction was 48.0 nm. The variation in crystallite size of nickel may be explained by the agglomeration and sintering of nanoparticles under high temperature [40] and may also result in the increase of surface area for reduced sample.

3.1.6. *Reducibility of catalysts*

The TPR profiles of the 20Ni/SiC-M catalysts are shown in Fig. 6. The H_2 consumption was gradually increased when temperature ramped from 350 °C, and a major reduction at around 420 °C was observed. A similar optimal reduction temperature was reported for other nickel-based supported catalyst, for example, Gao et al. observed a maximum reduction peak at around 420 °C for nano-NiO catalysts over α-Al_2O_3, and they suggested that the NiO particles were incorporate with the pores of ceramic support [34]. For the monolithic SiC ceramic support, it seems to have a similar reduction property compared with α-Al_2O_3, as the mean crystallite size of NiO nanoparticles were similar (36.4 nm vs 32.8 nm, respectively) in this work and Gao et al.'s work.

3.2. *Catalytic performance*

As the methane feeding was already diluted with nitrogen to form a 10% CH_4/N_2 mixture gas, there was no additional dilution of methane. The mixed gas flowrate and deionized water flowrate were adjusted to achieve the desired GHSV and steam to carbon ratio. The steam was carried by nitrogen flow to the main reactor when the reaction temperature was stable, and the mixture gas was introduced and replaced the pure nitrogen when the relative humidity of exhaust gas was without significant fluctuations.

A typical scenario of multi-gas measurement for the monolithic catalysts was shown in Fig. 7, including multiple phases: (1) phase 1: steam generation and stabilisation, by the end of phase 1, the mixture gas of methane and nitrogen was used at carrier gas; (2) phase 2: dynamic reaction, gas compositions turned to be stable; (3) phase 3: steady state, data was collected; (4) phase 4: post-reaction and purging. The steady state was reached at the reaction temperature within tens of seconds and stayed steadily for all gas compositions. Similar results were obtained for different operating temperatures and with different batch of monolithic catalysts.

3.2.1. *Effect of gas hourly space velocity (GHSV)*

Gas hourly space velocity (GHSV) is a key factor in judging scale up potential for industrial applications of new catalysts. It is defined by the ratio of gas rate per unit of catalyst, higher GHSV's tend to lead to lower conversion rates as they lower the residence time of the gas in the system, however, they crucially increase the reactor throughput meaning higher overall production rates. As shown in Eq. (9), GHSV is calculated based on volumetric gas flow rate per hour divided by the volume of catalysts.

$$\mathrm{GHSV}\left(\mathrm{h}^{-1}\right) = \frac{\sum \mathrm{Q_i}}{\mathrm{V_{catalyst}}} (\mathrm{i} = \mathrm{CH_4}, \mathrm{H_2}, \mathrm{CO_2}, \mathrm{CO}, \mathrm{N_2}) \quad (9)$$

To achieve a different GHSV value, the feed rate of water and methane/nitrogen mixture gas were adjusted to maintain the steam to carbon ratio of 3. Fig. 8 shows the results for the comparison for four GHSV values (10,000 h^{-1}, 15,000 h^{-1}, 20,000 h^{-1}, 25,000 h^{-1}) using the monolithic catalyst 20Ni/SiC-M operating at 600 °C.

It can be observed that methane conversion and hydrogen yield became lower when GHSV values rose, as lower GHSV value means longer contact time for the reactants over the same number of active sites. Methane conversion increased 15% to reach a high level of 77% for a GHSV value of 10,000 h^{-1}, meanwhile, hydrogen yield increased by 15% points to reach 65%. When GHSV value was set to 10,000 h^{-1}, a high CO selectivity of about 55% was also observed, and it reduced significantly when GHSV became greater. Hydrogen selectivity did not have significant variation, as it stayed around 77% for all GHSV values.

The thermodynamic equilibrium was calculated using FactSage™, assuming in a batch reactor, 3 mol of steam and 1 mol of methane was introduced under a total pressure of 1 bar. The methane conversion, hydrogen yield at 600 °C were found 77.2%, 70.0%, respectively. In

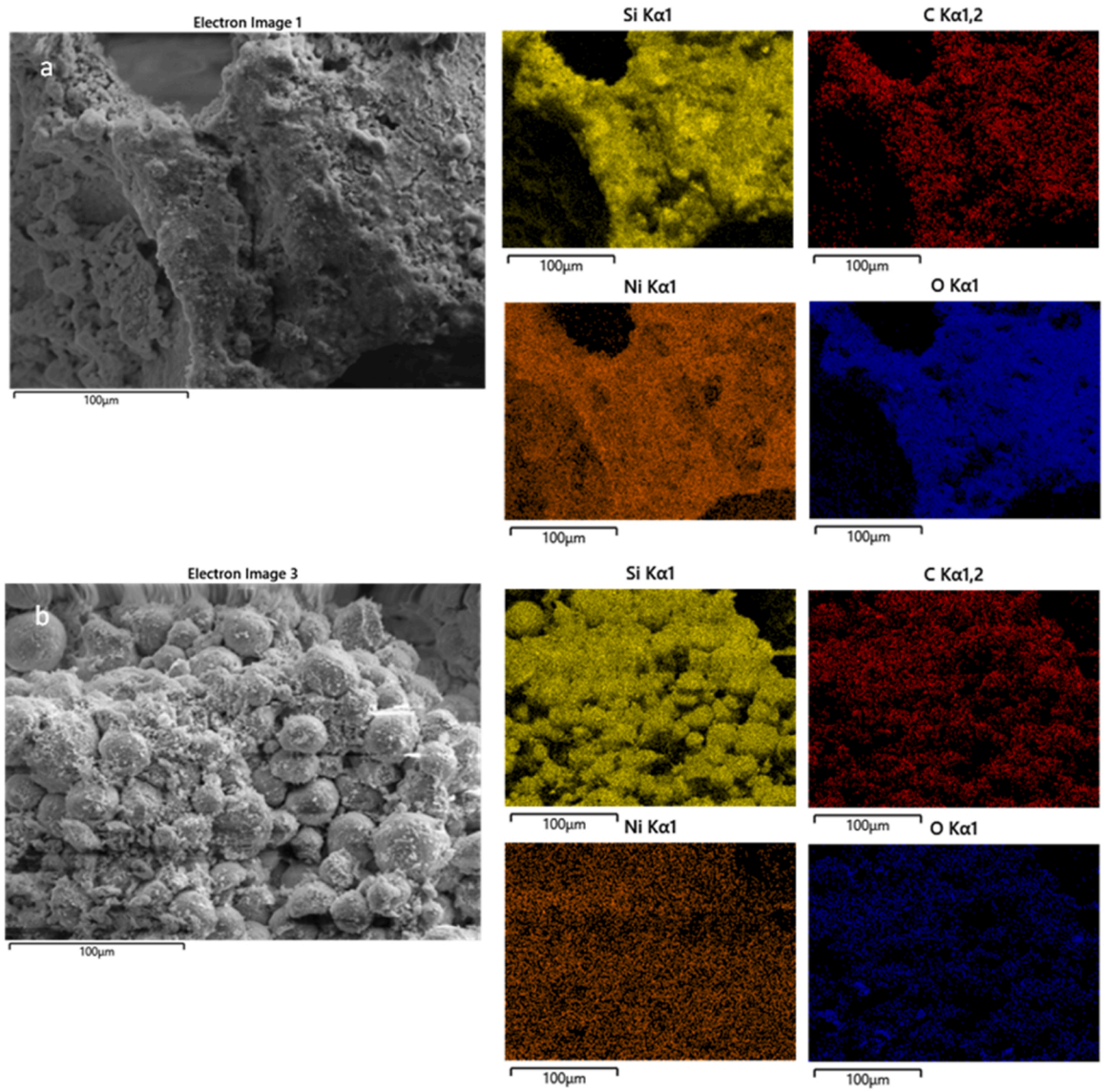


Fig. 4. SEM-EDS results of (a) fresh catalyst 20Ni/SiC-M and (b) used catalyst 20Ni/SiC-M.

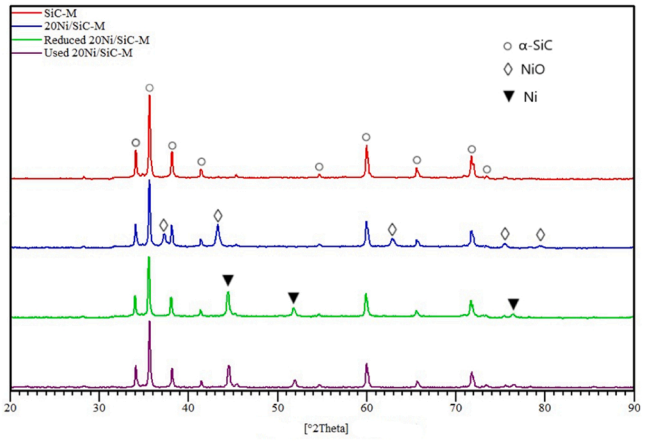


Fig. 5. XRD patterns of SiC-M, fresh, reduced and used 20Ni/SiC-M catalysts.

fact, the GHSV value is zero for this thermodynamic equilibrium scenario, and the 20Ni/SiC-M catalysts exhibited a thermodynamic-level performance for carbon conversion, and it is not worthy decreasing GHSV further to get closer to equilibrium as it would only achieve a minor improvement.

The GHSV describes how fast the gaseous reactants passed through the catalytic monolith, at higher GSHV's, the residence time is lower and there will be less chance that the active sites on surface of the material were used as there was a reduced frequency of successful collisions, and unreacted gas will pass through unreacted. This can explain the increasing of carbon conversion when GHSV was reduced, as more methane and steam molecules reacted over a longer contact time. Esteves et al. studied the influence of space velocity for methane decomposition reaction over CoMo/MgO catalyst, and they found the similar trends for methane conversion as the contact time between gas and catalyst were small when space velocity was high [41]. The final state of carbon and hydrogen is contingent on the balance between SMR and WGS (Eqs. (1) and (2)) and the properties of catalysts. The selectivity of hydrogen and carbon monoxide (CO) depends not only on the final state of carbon and hydrogen but also the methane conversion. The hydrogen selectivity will not be shown a significant variation when hydrogen is the predominant gas in exhaust gas, as similar scenario was

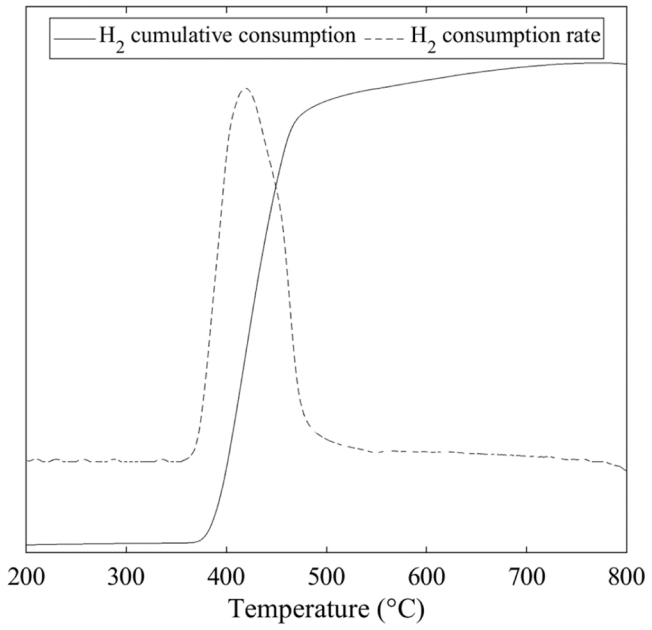


Fig. 6. Temperature Programmed Reduction (TPR) showing hydrogen consumption and consumption rates for 20Ni/SiC catalysts for a temperature range from 200° to 800°C.

shown in Fig. 8, and that explains the similar hydrogen selectivity value for all GHSVs. Theoretically, CO gas was easier exhausted and less amount of carbon was converted to CO_2 via WGS, as GHSV values increased. This contradicted the results of CO selectivity of 20Ni/SiC-M. However, the structural properties of monolithic catalysts may mitigate the effects of high speed of the gaseous materials, and as a result, increase the reactivity of SMR and WGS. Under high GHSV conditions (>15,000 h^{-1}), the impact of porous structure over CO selectivity seems to be important as the value remained approximately constant (around 48%). Therefore, 20Ni/SiC-M catalyst displayed a high catalytic efficiency of SMR when GHSV was at 10,000 h^{-1}, and the transportation of feed gases could benefit from its high gas permeability through its pores and channels.

3.2.2. *Effect of reaction temperature*

In order to evaluate the catalytic activities of a catalyst for the extreme conditions, a GHSV value of 20,000 h^{-1} was chosen. The results of conducted catalytic performance tests for all xNi/SiC-M catalysts (x = 2, 10, 20) are shown in Fig. 9, in terms of methane conversion vs temperature, hydrogen yield vs temperature, hydrogen selectivity vs temperature and carbon monoxide (CO) selectivity vs temperature. For all samples tested, 20Ni/SiC-M was chosen to evaluate the standard deviation of monoliths' structural and textural properties by three repetitions using different 20Ni/SiC-M catalysts.

These results highlight how the SiC monolithic catalysts perform under SMR conditions from 600 °C to 800 °C: both higher methane conversion and hydrogen yield were found when operating temperature rose. For the reference sample 20Ni/SiC-M, the highest methane conversion obtained was about 86% with a highest hydrogen yield of over 68%, both were observed at 800 °C. When the reaction temperature was between 650 °C and 750 °C, it seems to have a similar carbon conversion and hydrogen yield which was around 80% and 66%, respectively. These results were proved to be precise as the low standard deviations was obtained. The activities of 20Ni/SiC-M were not far from the equilibrium values, as the differences were 7–18% for methane conversions and 9–18% for hydrogen yields. The equilibrium data were obtained via FactSage software applying a batch condition with the presence of 1 mol of methane and 3 moles of steam under a total pressure of 1 bar.

When reaction temperature rose, hydrogen selectivity decreased slightly and the average value was around 78%. These data highly approached the equilibrium level. CO selectivity increased significantly from 48% to 76%, as reaction temperature rose from 600 °C to 800 °C. Since SMR reaction is endothermic, increasing the reaction temperature favours its mechanism and more CO were produced. In contrast, WGS reaction is exothermic so less CO_2 was produced when the temperature increased. Fig. 10 shows the average compositions for exhaust gas (CH_4, H_2, CO, CO_2) for the tests carried on with 20Ni/SiC-M. It can be observed that CO increased from 8% to 15% while CO_2 dropped from 9% to 5%, as temperature rose.

3.2.3. *Effect of metal loading on SiC-M*

Using the same GHSV value (20,000 h^{-1}) and steam to carbon ratio (3), a new series of catalyst performance tests was conducted with a fresh 10Ni/SiC-M catalyst. The results, in terms of methane conversion, hydrogen yield, hydrogen and CO selectivity were compared with previous results for 20Ni/SiC-M and also shown in Fig. 9.

It can be observed that the catalytic activity decreased when the nickel loading reduced, but their differences were not as significant as expected: only 5–9% for the comparison between 10Ni/SiC-M and 20Ni/SiC-M, and only 6–12% for the comparison between 2Ni/SiC-M and 10Ni/SiC-M, in terms of methane conversions. For hydrogen yield, only 2–5% when 10Ni/SiC-M compared with 20Ni/SiC-M, and only 9–16%

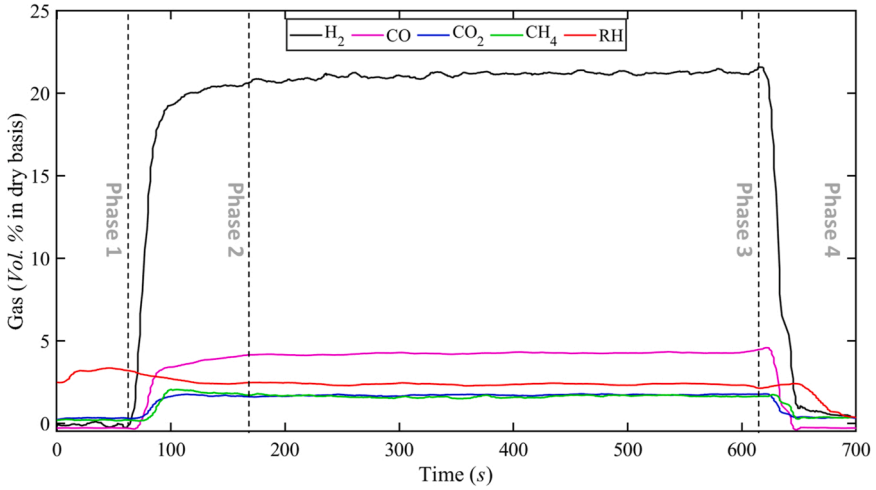


Fig. 7. Gas composition of exhaust gas for 20Ni/SiC-M (raw output) showing different phases of reaction at 700 °C.

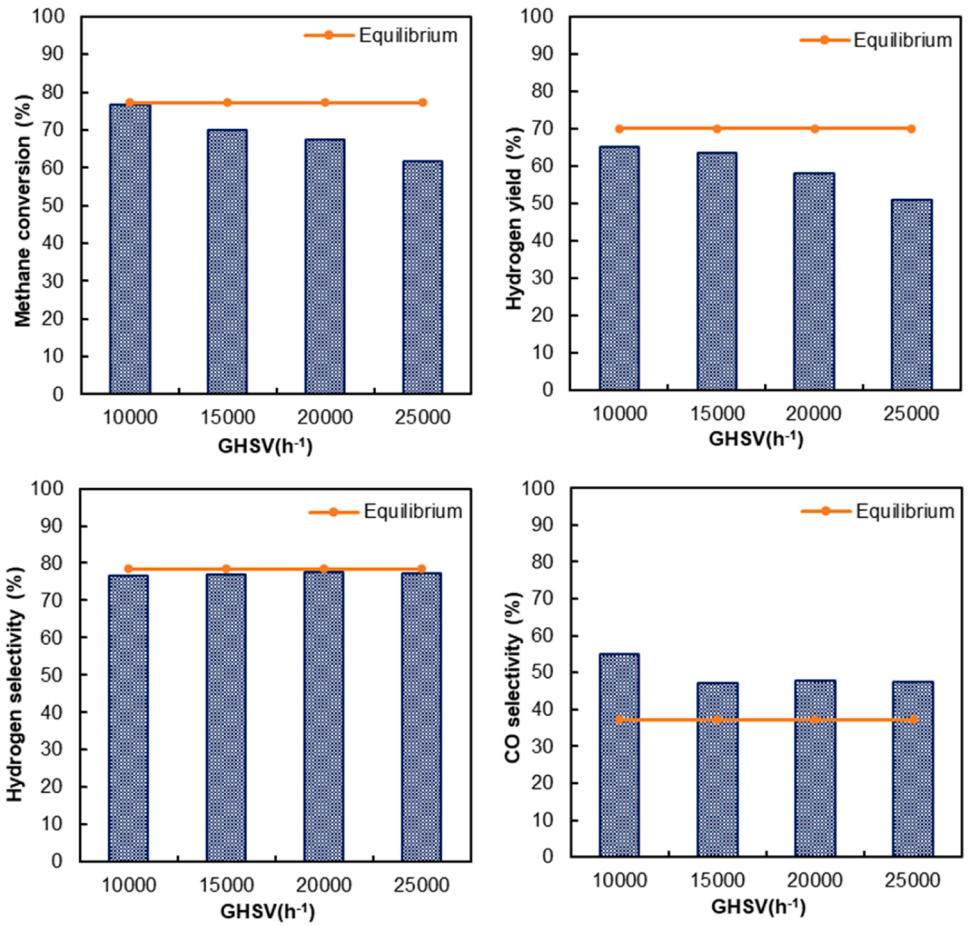


Fig. 8. Catalytic performances of 20Ni/SiC-M at 600 °C, S:C = 3, under different GHSV's (a) methane conversion, (b) hydrogen yield, (c) hydrogen selectivity, and (d) CO selectivity.

when 2Ni/SiC-M compared with 10Ni/SiC-M. The observed trend can be understood, as lower nickel loading means less available active sites on surface, with increasing number of active sites, the reaction rate boosts, results in a high catalytic activity [42]. Herein, it would be much more difficult for methane or steam molecules to occupy the sites properly and reduces the frequency of potential successful collisions when there were less available sites. However, from this data it seems that the adsorption of reactants wasn't influenced strongly as the number of sites reduced, which could be because of the unsaturated occupation of available actives sites during the tests under severe operating conditions. Even though the active sites on 2Ni/SiC-M catalyst were much fewer than 20Ni/SiC-M, as lower catalyst loading means a better dispersion of nanoparticles on the surface [43], the contact time for the gas mixture reacted over these sites was limited and many sites on surface of 20Ni/SiC-M were activated but stay unused. This work shows that a loading of only 2 wt% of nickel crystallites can achieve a methane conversion of 55–69% and reach 45–57% for hydrogen yield. Khzouz et al. tested a commercial Ni/Al_2O_3 catalyst (nickel loading at 40%) and they found a methane conversion of 78.2% under 600 °C, steam to carbon ratio of 3 and 25 mL/min of pure methane [44]. It can be seen in Khzouz et al.'s work that the extremely high loading of nickel and the low gas velocity does lead to a higher methane conversion but doesn't necessarily represent realistic operating conditions or significantly greater catalytic activity.

In terms of hydrogen selectivity, only minor differences for different nickel loading were found at lower temperature (600–700 °C), which was around 78%; as nickel loading was reduced the hydrogen selectivity was slightly decreased when reaction temperature was high (750–800 °C). The same trend of CO selectivity versus temperature was found for monolith catalysts with different metal loadings. As the nickel loading reduced, CO selectivity was reduced and approached the equilibrium level. The CO selectivity at equilibrium reveals the CO and CO_2 ratio thermodynamically with the absence of catalysts. It seems to demonstrate that the high content of catalysts on Ni/SiC-M had high selectivity on SMR reaction (Eq. (1)). More available active sites can produce more CO gas via SMR, so catalysts with high nickel loading can covert more carbon to CO rather than CO_2, resulting in a high CO selectivity. When the nickel loading was extremely low, a CO selectivity at equilibrium level was theoretically expected as it minimised the influence of catalysts over the two reactions involved, SMR and WGS (Eqs. (1) and (2)).

3.3. Comparison of catalytic performance

Focusing on steam reforming of methane, the performance of 20Ni/SiC-M catalyst presented in this work was compared with literature, shown in Table 4.

The data reported in Table 4 highlights the optimal performance of the structured SiC monolithic catalyst in terms of methane conversion, compared with other structured SiC catalysts studied previously. The 20Ni/SiC-M has a better performance, as the other catalysts can achieve their best activity at lower GHSV conditions or higher temperature. For example, Palma et al. [21] tested a commercial catalyst ($Katalco_{JM}$ Quadralobe) and their honeycombs catalysts at same operating conditions (600 °C, S:C=3, GHSV=25,000 h^{-1}). The methane conversion was relatively low, compared with 20Ni/SiC-M (40% for commercial catalyst, 20% for honeycomb catalyst, 60% for 20Ni/SiC-M). The 20Ni/SiC-M catalyst can perform highly efficiently at low temperatures

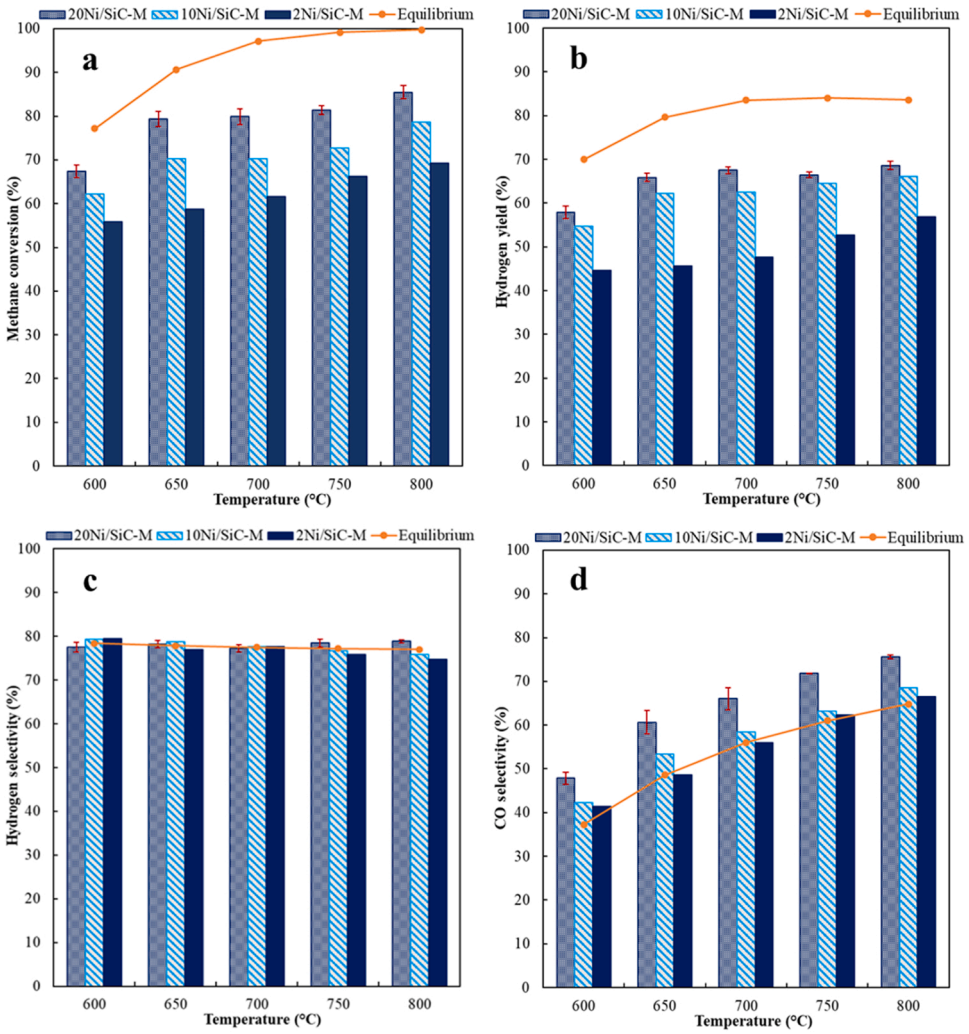


Fig. 9. Catalytic performances of 20xNi/SiC-M (x = 2, 10, 20) at S:C = 3 at different temperatures, (a) methane conversion, (b) hydrogen yield, (c) hydrogen selectivity, and (d) CO selectivity.

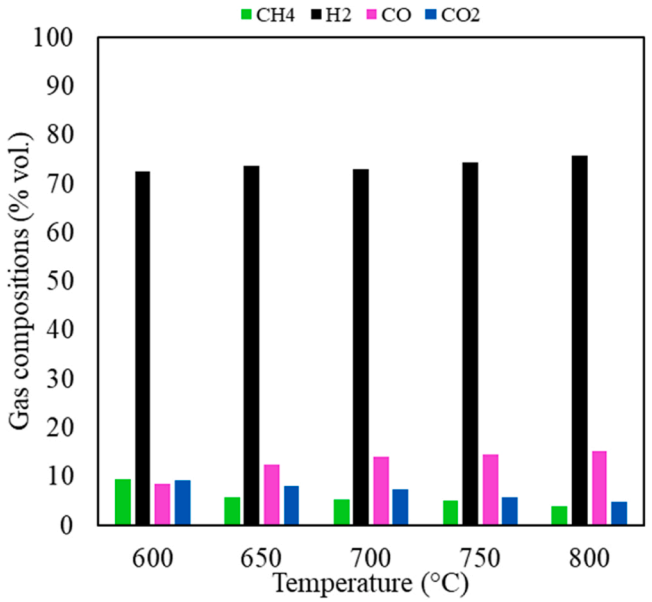


Fig. 10. Gas compositions for 20Ni/SiC-M at S:C = 3 and GHSV = 20,000 h^{-1} over a range of temperatures, presented on a water and nitrogen free basis.

(600–650 °C), as the equilibrium conversion was reached under a moderate operating condition (600 °C, GHSV=10,000 h^{-1}), while others can achieve a lower methane conversion (65% vs. 79%) at similar conditions (GHSV: 30,000 h^{-1} vs. 20,000 h^{-1}, 650 °C, S:C=3) [1].

4. Conclusions

Structured monolithic SiC catalysts with 2–20 wt% of nickel loading were prepared by a modified freeze-gelation and wet impregnation methods. Catalytic performance tests at severe but realistic conditions (10,000–25,000 h^{-1} of GHSV, 1 bar of pressure and 10% CH_4 balanced with N_2 as the feed) were performed in the temperature range of 600–800 °C. The results showed that the 20Ni/SiC-M catalysts exhibited a high catalytic activity, especially at low SMR temperatures, compared with other SiC supported nickel-based catalysts. It achieved CH_4 equilibrium conversion at 600 °C, S:C= 3, GHSV= 10,000 h^{-1}. The structural and textural properties of the SiC-M catalyst support, such as porosity, had a positive effect on mass and heat transfer which contributed to its excellent performance at low operating temperature. There are still some challenges focusing on the deactivation of the catalysts as nickel-based catalysts were reported to suffer from coke formation [45]. Long-term test regarding with the investigation of catalyst stability and coke resistance are still interesting to be carried out, to better understand how close to the real Ni/SiC-M applications. Furthermore, this catalytic monolith had the advantage of being light,

Table 4
Comparison of different Ni-based structured SiC catalysts performance in SMR.

Catalyst and support	Operating conditions covered in article	Catalyst performance under optimal conditions	Reference
5% Ni on 19% CeO_2 wash-coated commercial β-SiC honeycombs	T: 500–850 °C P: 1 atm, S/C: 3.0 GHSV: 6250, 25,000 h^{-1}	X_{CH4} = 90% at 850 °C, 6250 h^{-1}	[21,22]
10% Ni on SiC modified (Calcium aluminate) boehmite granules (1–1.5 mm)	T: 650–850 °C P: 1 atm, S/C: 1.0 and 3.0 GHSV: 30,000 h^{-1}	X_{CH4} = 97.7% at 850 °C, 30,000 h^{-1}	[1]
Ni/SiC@Al_2O_3 core-shell powders (Ni % = 18.8%)	T: 600 °C P: 1 atm, S/C: 3.5 F/W = 137,000 mL h^{-1} g_{cat}^{-1}	X_{CH4} = 78% at 600 °C	[23]
15% Ni on 19%CeO_2 wash-coated commercial SiC honeycombs	T: 550–950 °C P: 1 atm, S/C: 3.0 GHSV: 3300, 5000 h^{-1}	CH_4 equilibrium conversion at 800 °C, 3300 h^{-1} and 850 °C, 5,000 h^{-1}	[24]
7%Ni on 19% CeO_2 wash-coated commercial SiC honeycombs	T: 550–800 °C P: 1 atm, S/C: 3.0 GHSV: 5,000 h^{-1}	CH_4 equilibrium conversion at 750 °C, 5,000 h^{-1}	[25]
20Ni/SiC-M	T: 600–800 °C P: 1 bar, S/C: 3.0 GHSV: 10,000, 15,000, 20,000 h^{-1}	CH_4 equilibrium conversion at 600 °C, 10,000 h^{-1} X_{CH4} = 86% at 800 °C, 20,000 h^{-1}	This work

strong, and yet very stable in aggressive high temperature applications, and shows promise for future clean hydrogen production.

Funding sources

This research did not receive any specific grant from funding agencies in the public, commercial, or not-for-profit sectors.

CRediT authorship contribution statement

Shen Ziqi: Conceptualization, Formal analysis, Investigation, Methodology, Visualization, Writing – original draft. **Clough Peter:** Conceptualization, Methodology, Project administration, Supervision, Writing – review & editing. **Nabavi Ali:** Conceptualization, Methodology, Supervision, Writing – review & editing.

Declaration of Competing Interest

The authors declare that they have no known competing financial interests or personal relationships that could have appeared to influence the work reported in this paper.

Acknowledgements

The authors wish to thankfully acknowledge Dr. David Danaci and Dr. Jose Juan Morales Corona for their help performing MIP characterisation.

References

[1] Y.S. Noh, K.Y. Lee, D.J. Moon, Hydrogen production by steam reforming of methane over nickel based structured catalysts supported on calcium aluminate modified SiC, Int J. Hydrog. Energy 44 (2019) 21010–21019, https://doi.org/10.1016/j.ijhydene.2019.04.287.
[2] International Energy Agency, Global Hydrogen Review 2022, 2022.
[3] Howard F. Rase, Handbook of Commercial Catalysts: Heterogeneous Catalysts, 2000.
[4] Drnevich Raymond Francis, Papavassiliou Vasilis, Steam Methane Reforming Method, WO2006055326A1, 2006.
[5] P.P.S. Quirino, A.F. Amaral, F. Manenti, K. v Pontes, Mapping and optimization of an industrial steam methane reformer by the design of experiments (DOE), Chem. Eng. Res. Des. 184 (2022) 349–365, https://doi.org/10.1016/j.cherd.2022.05.035.
[6] E. Meloni, M. Martino, V. Palma, A short review on ni based catalysts and related engineering issues for methane steam reforming, Catalysts 10 (2020), https://doi.org/10.3390/catal10030352.
[7] R.D. Alli, P.A.L. de Souza, M. Mohamedali, L.D. Virla, N. Mahinpey, Tri-reforming of methane for syngas production using Ni catalysts: current status and future outlook, Catal. Today 407 (2023) 107–124, https://doi.org/10.1016/j.cattod.2022.02.006.
[8] S. Wang, S.A. Nabavi, P.T. Clough, A review on bi/polymetallic catalysts for steam methane reforming, Int J. Hydrog. Energy (2023), https://doi.org/10.1016/j.ijhydene.2023.01.034.
[9] A. Arman, F.Y. Hagos, A.A. Abdullah, R. Mamat, A.R.A. Aziz, C.K. Cheng, Syngas production through steam and CO_2 reforming of methane over Ni-based catalyst-A Review, in: IOP Conf Ser Mater Sci Eng, 736, Institute of Physics Publishing, 2020, https://doi.org/10.1088/1757-899X/736/4/042032.
[10] M. Wang, X. Tan, J. Motuzas, J. Li, S. Liu, Hydrogen production by methane steam reforming using metallic nickel hollow fiber membranes, J. Membr. Sci. 620 (2021), https://doi.org/10.1016/j.memsci.2020.118909.
[11] F. Kapteijn, J.A. Moulijn, Structured catalysts and reactors – Perspectives for demanding applications, Catal. Today 383 (2022) 5–14, https://doi.org/10.1016/j.cattod.2020.09.026.
[12] M.V. Twigg, J.T. Richardson, Theory and applications of ceramic foam catalysts, Chem. Eng. Res. Des. 80 (2002) 183–189, https://doi.org/10.1205/026387602753501906.
[13] Cybulski A., Moulijn J.A. , Modelling of Heat Transfer in Metallic Monoliths Consisting of Sinusoidal Cells, 49, 1994.
[14] A.R. Keshavarz, M. Soleimani, Nano-sized Ni/(CaO)x-(Al2O3)y catalysts for steam pre-reforming of ethane and propane in natural gas: The role of CaO/Al2O3 ratio to enhance conversion efficiency and resistance to coke formation, J. Nat. Gas Sci. Eng. 45 (2017) 1–10, https://doi.org/10.1016/j.jngse.2017.05.019.
[15] M.J. Ledoux, C. Uong Pham-Huu, R.R. Ghianellit, Catalysis with carbides, Solid State Mater. Sci. (1996) 96–100.
[16] J.M. García-Vargas, J.L. Valverde, A. de Lucas-Consuegra, B. Gómez-Monedero, P. Sánchez, F. Dorado, Precursor influence and catalytic behaviour of Ni/CeO 2 and Ni/SiC catalysts for the tri-reforming process, Appl. Catal. A Gen. 431–432 (2012) 49–56, https://doi.org/10.1016/j.apcata.2012.04.016.
[17] R. Pérez-Hernández, G. Mondragón-Galicia, A. Allende Maravilla, J. Palacios, Nano-dimensional CeO2 nanorods for high Ni loading catalysts: H2 production by autothermal steam reforming of methanol reaction, Phys. Chem. Chem. Phys. 15 (2013) 12702–12708, https://doi.org/10.1039/c3cp52032c.
[18] W. Nabgan, T.A.T. Abdullah, R. Mat, B. Nabgan, Y. Gambo, K. Moghadamian, Acetic acid-phenol steam reforming for hydrogen production: effect of different composition of La2O3-Al2O3 support for bimetallic Ni-Co catalyst, J. Environ. Chem. Eng. 4 (2016) 2765–2773, https://doi.org/10.1016/j.jece.2016.05.030.
[19] M. Araque, L.M. Martínez T, J.C. Vargas, A.C. Roger, Hydrogen production by glycerol steam reforming over CeZrCo fluorite type oxides, Catal. Today 176 (2011) 352–356, https://doi.org/10.1016/j.cattod.2010.11.066.
[20] Shekhar R. Kulkarni, Vijay K. Velisoju, Fernanda Tavares, Alla Dikhtiarenko, Jorge Gascon , Pedro Castaño. Silicon carbide in catalysis: from inert bed filler to catalytic support and multifunctional material, Catalysis Reviews, 2022.
[21] V. Palma, A. Ricca, M. Martino, E. Meloni, Innovative structured catalytic systems for methane steam reforming intensification, Chem. Eng. Process. Process.Intensif. 120 (2017) 207–215, https://doi.org/10.1016/j.cep.2017.07.012.
[22] V. Palma, M. Martino, E. Meloni, A. Ricca, Novel structured catalysts configuration for intensification of steam reforming of methane, Int J. Hydrog. Energy 42 (2017) 1629–1638, https://doi.org/10.1016/j.ijhydene.2016.06.162.
[23] H. Lee, D. Lee, Synthesis chemistry and properties of ni catalysts fabricated on sic@al2o3 core-shell microstructure for methane steam reforming, Catalysts 10 (2020), https://doi.org/10.3390/catal10040391.
[24] E. Meloni, M. Martino, A. Ricca, V. Palma, Ultracompact methane steam reforming reactor based on microwaves susceptible structured catalysts for distributed hydrogen production, Int J. Hydrog. Energy 46 (2021) 13729–13747, https://doi.org/10.1016/j.ijhydene.2020.06.299.
[25] E. Meloni, M. Martino, V. Palma, Microwave assisted steam reforming in a high efficiency catalytic reactor, Renew. Energy 197 (2022) 893–901, https://doi.org/10.1016/j.renene.2022.07.157.
[26] Christian, M. Mitchell, P.J.A. Kenis, Ceramic microreactors for on-site hydrogen production from high temperature steam reforming of propane, Lab Chip 6 (2006) 1328–1337, https://doi.org/10.1039/b607552e.
[27] K.S. Park, M. Son, M.J. Park, D.H. Kim, J.H. Kim, S.H. Park, et al., Adjusted interactions of nickel nanoparticles with cobalt-modified MgAl2O4-SiC for an enhanced catalytic stability during steam reforming of propane, Appl. Catal. A Gen. 549 (2018) 117–133, https://doi.org/10.1016/j.apcata.2017.09.031.
[28] S. Fukahori, H. Koga, T. Kitaoka, A. Tomoda, R. Suzuki, H. Wariishi, Hydrogen production from methanol using a SiC fiber-containing paper composite impregnated with Cu/ZnO catalyst, Appl. Catal. A Gen. 310 (2006) 138–144, https://doi.org/10.1016/j.apcata.2006.05.032.
[29] M. Liao, C. Guo, W. Guo, T. Hu, H. Qin, P. Gao, et al., Hydrogen production in microreactor using porous SiC ceramic with a pore-in-pore hierarchical structure as catalyst support, Int J. Hydrog. Energy 45 (2020) 20922–20932, https://doi.org/10.1016/j.ijhydene.2020.05.244.

[30] S. Fukahori, H. Koga, T. Kitaoka, M. Nakamura, H. Wariishi, Steam reforming behavior of methanol using paper-structured catalysts: experimental and computational fluid dynamic analysis, Int J. Hydrog. Energy 33 (2008) 1661–1670, https://doi.org/10.1016/j.ijhydene.2007.12.063.
[31] V. Palma, C. Ruocco, F. Castaldo, A. Ricca, D. Boettge, Ethanol steam reforming over bimetallic coated ceramic foams: effect of reactor configuration and catalytic support, Int J. Hydrog. Energy 40 (2015) 12650–12662, https://doi.org/10.1016/j.ijhydene.2015.07.138.
[32] W. Guo, T. Hu, H. Qin, P. Gao, H. Xiao, Preparation and in situ reduction of Ni/SiCxOy catalysts supported on porous SiC ceramic for ethanol steam reforming, Ceram. Int. 47 (2021) 13738–13744, https://doi.org/10.1016/j.ceramint.2021.01.235.
[33] M. Fukushima, M. Nakata, Y. Zhou, T. Ohji, Y. ichi Yoshizawa, Fabrication and properties of ultra highly porous silicon carbide by the gelation-freezing method, J. Eur. Ceram. Soc. 30 (2010) 2889–2896, https://doi.org/10.1016/j.jeurceramsoc.2010.03.018.
[34] J.H. Eom, Y.W. Kim, S. Raju, Processing and properties of macroporous silicon carbide ceramics: a review, J. Asian Ceram. Soc. 1 (2013) 220–242, https://doi.org/10.1016/j.jascer.2013.07.003.
[35] P. de Wit, E.J. Kappert, T. Lohaus, M. Wessling, A. Nijmeijer, N.E. Benes, Highly permeable and mechanically robust silicon carbide hollow fiber membranes, J. Membr. Sci. 475 (2015) 480–487, https://doi.org/10.1016/j.memsci.2014.10.045.
[36] Ledoux M.J., Uong Pham-Huu C., Ghianellit R.R. , Catalysis with Carbides 1996.
[37] Forzatti P., Lietti L. , Catalyst Deactivation. 1999.
[38] Yoshimura M., Un-Ichiro Kase J., Somiya S. Oxidation of SiC Powder by High-temperature, High-pressure H 2 0, I. 1986.
[39] Z. Peng, C. mao Miao, W. Sun, Y. long Xu, H. kun Chen, Y. feng Liu, et al., High-temperature thermal stability of C/C-ZrC-SiC composites via region labeling method, Trans. Nonferrous Met. Soc. China (Engl. Ed.) 32 (2022) 3349–3361, https://doi.org/10.1016/S1003-6326(22)66024-2.
[40] J.T. Richardson, R. Scates, M.V. Twigg, X-ray diffraction study of nickel oxide reduction by hydrogen, Appl. Catal. A Gen. 246 (2003) 137–150, https://doi.org/10.1016/S0926-860X(02)00669-5.
[41] L.M. Esteves, A.A. Daás, H.A. Oliveira, F.B. Passos, Influence of space velocity and catalyst pretreatment on COx free hydrogen and carbon nanotubes production over CoMo/MgO catalyst, Int J. Hydrog. Energy 45 (2020) 27299–27311, https://doi.org/10.1016/j.ijhydene.2020.07.133.
[42] X. Li, H.J. Zhang, H. Li, C. Deng, J. Yang, Evaluation of loading influence on catalytic performance of co-based catalyst for oxygen reduction, ECS Electrochem. Lett. 3 (2014), https://doi.org/10.1149/2.0061409eel.
[43] S. Velu, S.K. Gangwal, Synthesis of alumina supported nickel nanoparticle catalysts and evaluation of nickel metal dispersions by temperature programmed desorption, Solid State Ion. 177 (2006) 803–811, https://doi.org/10.1016/j.ssi.2006.01.031.
[44] M. Khzouz, J. Wood, B. Pollet, W. Bujalski, Characterization and activity test of commercial Ni/Al2O 3, Cu/ZnO/Al2O3 and prepared Ni-Cu/Al 2O3 catalysts for hydrogen production from methane and methanol fuels, Int. J. Hydrog. Energy vol. 38 (2013) 1664–1675, https://doi.org/10.1016/j.ijhydene.2012.07.026.
[45] C.J. Liu, J. Ye, J. Jiang, Y. Pan, Progresses in the preparation of coke resistant Ni-based catalyst for steam and CO 2 reforming of methane, ChemCatChem 3 (2011) 529–541, https://doi.org/10.1002/cctc.201000358.



https://dspace.org/

Design and performance testing of a monolithic nickel-based SiC catalyst for steam methane reforming

Shen, Ziqi; Nabavi, Seyed Ali; Clough, Peter T.

2024-01-25
Elsevier
https://doi.org/10.1016/j.apcata.2023.119529
Shen Z, Nabavi SA, Clough PT. (2024) Design and performance testing of a monolithic nickel-based SiC catalyst for steam methane reforming. Applied Catalysis A: General, Volume 670, January 2024, Article number 119529

Downloaded from a DSpace repository. https://dspace.org/